STUDY OF BISTATIC RADAR TRANSMISSION GEOMETRIES FOR CHARACTERIZING ASTEROID INTERIORS. M. S. Haynes[1], A. Herique[2], I. Fenni[1], B. Davidsson[1], C. Raymond[1], P. Michel[3], [1]Jet Propulsion Laboratory, California Institute of Technology (4800 Oak Grove Dr. M/S 300-235, Pasadena, CA. mark.s.haynes@jpl.nasa.gov), [2]Univ. Grenoble Alpes, CNRS, CNES, IPAG, Grenoble, France, [3]Université Côte d'Azur, Observatoire de la Côte d'Azur, CNRS, Laboratoire Lagrange, Nice, France

Introduction: Low-frequency radar transmission measurements of solar system small bodies were pioneered by the Rosetta-CONSERT instrument which made limited bistatic measurements of comet 67P/C-G, [1]. CONSERT was a radio transponder (90 MHz) that provided the two-way time of flight between the Rosetta orbiter and Philae lander. The time of flight was used to estimate the average real part of the relative dielectric constant of about 1.2, [2]. This value corroborated with the low bulk density [3] indicating extremely porous material with high dust to ice ratio and refractory fraction dominated by carbonaceous materials [2]. In general, low-frequency (5-100 MHz) radar transmission measurements are a simple and effective method to characterize bulk dielectric properties of small body interiors and infer information on both composition and internal structure [4].

The advent of small spacecraft, particularly cubesats, will enable multi-spacecraft observation geometries around solar system small bodies. The use of a cubesat for monostatic small body radar imaging will be demonstrated in ESA's Hera mission with the low-frequency radar JuRa that will image the interior of asteroid Didymorphos, [5]. Future small body radar imaging systems are envisioned with two or more small spacecraft or cubesats that orbit the body and collect arbitrary bistatic or bistatic transmission measurements through the body. Antipodal orbit geometries have been studied in [6].

We study three aspects of bistatic radar transmission measurements of asteroid interiors: 1) diffraction effects that constrain antipodal altitudes, 2) orbit altitudes that take advantage of natural lensing, and 3) estimating the average dielectric from time-of-flight with statistical spread due to scattering from heterogeneous dielectrics. The purpose of this work is to develop simple analysis methods to inform future instrument and mission design.

Diffraction Effects and Maximum Orbit Altitude: Bistatic transmission measurements require the body to be between two radar sensors and antipodal geometries are a subset of all possible bistatic transmission angles, [7]. Ideally, the path through the body can be treated as a dielectric slab from which inversion via time-of-flight is easily formulated. However, asteroids with diameters of 100s of meters are small enough that radar signals diffract around the

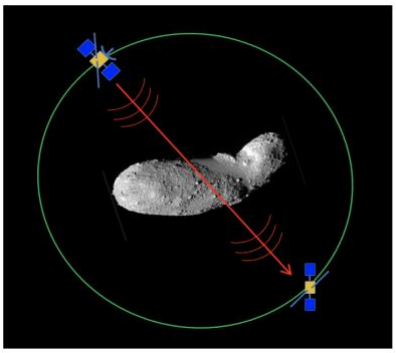

Figure 1: Illustration of bistatic radar transmission at an asteroid between two orbiting spacecraft.

outside and can interfere with the transmitted signal. Diffraction therefore can constrain the maximum orbit altitude for cleanly separated diffracted and transmitted signals. Lander-lander or orbit-lander (e.g., CONSERT) configurations provide the best shadowing for transmission, while far-field plane-wave incidence leads to interference.

We assess the maximum orbit altitude to achieve well-separated diffracted and transmitted signals in an antipodal geometry using time-domain scattering from a large dielectric sphere. A perfect sphere is worst-case diffraction because of its smoothness and homogeneity. Realistic asteroids will be non-spherical, rough, heterogenous, and lossy, therefore some diffraction effects will be present and 3D full-wave simulation of realistic models is needed for a complete assessment.

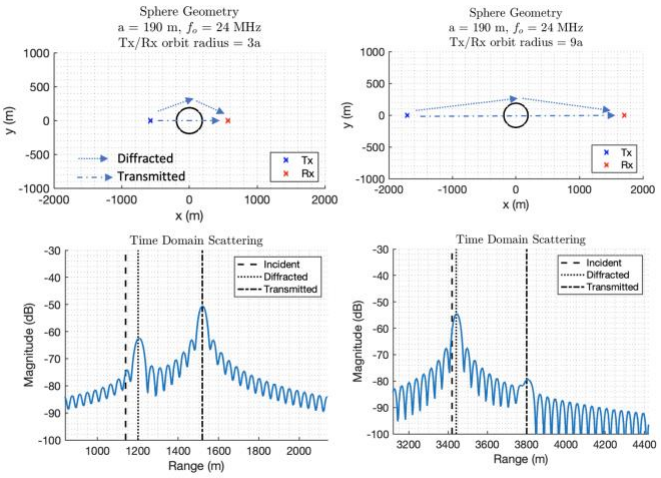

Figure 2: (top) Geometry for antipodal transmitter and receiver around a sphere. (bottom) Time-domain scattering from a sphere.

Figure 2 shows noiseless range-compressed co-polarized signals for antipodal transmission though a dielectric sphere. The radius is a=190m with dielectric constant ε_r=4+i0.04 and center frequency 24 MHz (20-28 MHz band). Vertical lines are the expected range of incident (no object), diffracted, and transmitted signals. For R=3a transmission is stronger than diffraction, while for R=9a transmission is swamped by the side-lobes of the diffracted signal which is indistinguishable from the incident field. A parametric study revealed orbit radii of R=2a-4a yield clean transmission signals, while R=10a is a reasonable maximum altitude. These results scale with frequency and body diameter, but lower orbits of a few body radii are desirable.

Lensing Effects and Orbit Trajectories: Bistatic configurations other than pure antipodal allows us to consider information content of the waves propagated throughout the body. A body with limited heterogeneity (e.g., aggregate of small blocks, or voids filled with sand) will act like an imperfect lens. Thus, for a given transmitter position, the signal is gathered on a limited sector: the angular aperture of this sector decreases with increasing altitude and is limited by caustics that are difficult to analyze. Low orbits allow better sampling of spreading wavefronts and thus better measurement of small variations in signal intensity and delay that carry information about interior heterogeneity. In general, a diversity of bistatic angles is important to fill out of the k-space of 3D SAR, [7]. Trajectories of both crafts should be chosen to maximize the number of geometric configurations in the asteroid frame to obtain the theoretical resolution.

Dielectric Estimation and Scattering Statistics: Estimating the average dielectric constant with time-of-flight measurements is a statistical process due to heterogeneity, noise, and instrument imperfections (for CONSERT see [8,9]). We study scattering effects in 2D. The asteroid model and Method of Moments-Characteristic Basis Function Method (MoM-CBFM) simulator are described in [10]. We simulate antipodal time-domain echoes at 5 MHz (4-6 MHz band) and 1.5^o steps. The body has $<\varepsilon_r>$=2.71, peak ε_r=4. The differential range (time-of-flight) between the predicted incident field and simulated transmitted field is used with body diameter to invert ε_r along each ray.

Figure 3 shows an example of this process: a) geometry and test object, b) time domain pulse for one transmission, c) set of antipodal transmission echoes from 0-180 degrees, and d) histogram of the estimated dielectric values from all paths. The mean estimated $<\varepsilon_r>$=2.55 with variance 0.7, therefore, for these parameters, a relative estimation uncertainty in $<\varepsilon_r>$ of

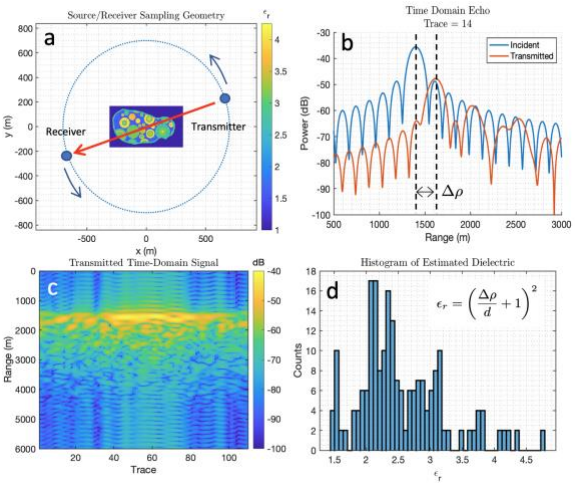

Figure 3: Simulated dielectric estimation using transmission measurements in 2D.

5% could be achieved with 25 independent samples assuming no other sensor errors.

Conclusions and Future Work: We analyzed diffraction effects and dielectric inversion in antipodal radar measurement geometries for solar system small bodies. Future work will explore general bistatic angles with 3D asteroid models, e.g., Figure 4 shows a 190m 3D rubble pile model of dielectric spheres with larger spheres on the exterior. Backscatter was simulated at 20 MHz using MoM-CBFM on the JPL Gattaca cluster; time-domain echoes are planned next.

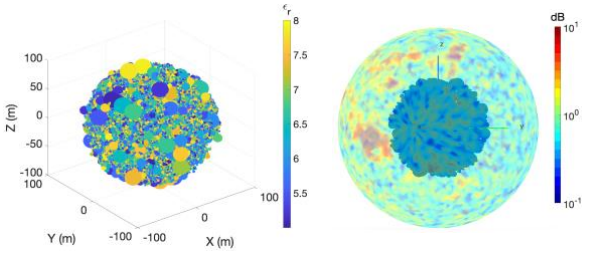

Figure 4: Left – Rubble pile model of dielectric spheres. Right – Radar backscatter efficiency at 20 MHz.

Acknowledgments: This research was done in part at the Jet Propulsion Laboratory, California Institute of Technology, under a contract with NASA (80NM0018D0004). ©2022. All right reserved. A.H. and P.M. acknowledge the French space agency CNES.

References: [1] Kofman, W., et al. (2007) *SSR 128*(1-4), 413–432. [2] Herique, A., et al (2016) *MNRA Soc*. 462, S516–S532. [3] Jorda, L., et al. (2016) *Icarus* 277, 257. [4] Herique, A., et al. (2018) *ASR* 62 2141-2162. [5] Herique, A., et al (2020) *EPSC* 2020-595. [6] S. Hernandez, et al. (2021) *AAS* 21-728. [7] Haynes, M., et al. (2021) *ASR* 68, 3903-3924. [8] Kofman, W., et al. (2015) AAAS 349, 6247. [9] Herique, A., et al., (1999) PSS, 47, 885-904. [10] Haynes, M., et al. (2021) *LPSC* 2548.